

Spatial arrangement and density variations in the cell envelope of *Deinococcus radiodurans*

Domenica Farci ^{a,b} and Dario Piano ^{a,b}

^aDepartment of Plant Physiology, Warsaw University of Life Sciences – SGGW, Warsaw, Poland; ^bDepartment of Life and Environmental Sciences, Università degli Studi di Cagliari, Cagliari, Italy

Corresponding authors: **Domenica Farci** (email: domenica.farci@unica.it); **Dario Piano** (email: dario.piano@unica.it)

Abstract

The cell envelope of the poly-extremophile bacterium *Deinococcus radiodurans* is renowned for its highly organized structure and unique functional characteristics. In this bacterium, a precise regularity characterizes not just the S-layer, but it also extends to the underlying cell envelope layers, resulting in a dense and tightly arranged configuration. This regularity is attributed to a minimum of three protein complexes located at the outer membrane level. Together, they constitute a recurring structural unit that extends across the cell envelope, effectively tiling the entirety of the cell body. Nevertheless, a comprehensive grasp of the vacant spaces within each layer and their functional roles remains limited. In this study, we delve into these aspects by integrating the state of the art with structural calculations. This approach provides crucial evidence supporting an evolutive pressure intricately linked to surface phenomena depending on the environmental conditions.

Key words: cell envelope, cell envelope complexes, extremophile, radiation resistance, *Deinococcus radiodurans* R1

Introduction

Deinococcus radiodurans is an ancient bacterium attributed to be as old if not older than the 10 phylogenetic lineages of eubacteria (Woese et al. 1985). Discovered in 1956 by Anderson and co-workers (Anderson et al. 1956), *D. radiodurans* has been taxonomically defined only in the early 80s (Brooks and Murray 1981), and its family, the *Deinococcaceae*, has been accurately described in decades of work by Robert G.E. Murray (Murray 1992) and collaborators. Murray's decades-long dedication to the comprehensive study of the poly-extremophile bacterium *D. radiodurans* provided an outstanding scientific legacy that contributed to our understanding of this remarkable organism. *Deinococcus radiodurans* cells exhibit a characteristic spherical shape and divide along two distinct planes, resulting in the formation of pairs and tetrads. Cell divisions, known as septa, develop from both sides of the cell (Murray et al. 1983; Floc'h et al. 2019). This microorganism is non-motile and lacks distinct resting forms. Regarding its cell envelope, *D. radiodurans* is classified as a Gram-negative that might exhibit Gram-positive staining characteristics. Additionally, within its family, it stands as one of the members distinguished by an external paracrystalline S-layer (Murray 1992). As many other representative strains of the *Deinococcus* genus, *D. radiodurans* is recognized for the remarkable capacity to endure doses of electromagnetic radiation, including ionizing gamma radiation, at extraordinary levels (Daly et al. 2004; Cox and Battista 2005; Daly 2023). Linked to this ability is its resistance to prolonged desiccation and possession of structures well suited to endure high temperatures

(Farci et al. 2016, 2018). This characteristic similarity aligns it closely with its “phylogenetic neighbor”, *Thermus thermophilus* (Oshima and Imahori 1974; Murray 1992). In recent years, the significance of the cell envelope has come to the forefront in contributing to these properties. This has also furnished crucial evidence regarding significant preventive and reparative mechanisms against adverse environmental factors (Farci et al. 2016, 2018, 2023a). Within this context, the highly organized cell envelope of this organism assumes a pivotal role, also supported by the widespread presence of xanthophylls, particularly deinoxanthin (Lemee et al. 1997; Tian et al. 2007, 2009, 2010; Ji 2010; Farci et al. 2016, 2022a, 2023a), and unique phosphoglycolipids (Anderson and Hansen 1985; Huang and Anderson 1989, 1991, 1995; Farci et al. 2022a, 2023a), both reported to be important in the resistance of the bacterium. On one hand, the cell envelope serves as a protective shield against potential environmental harm, encompassing not only electromagnetic stress but also extending to other forms of stress such as desiccation, elevated temperatures, and diverse mechanical stressors including pressure and vacuum (Farci et al. 2016, 2018; Ott et al. 2019). On the other hand, it also exhibits the ability to repair damage after it has occurred (Farci et al. 2023a). This latter trait has been particularly evident in instances of oxidative stress, linked to the mitigation of the effect induced by reactive oxygen species (ROS) formed after exposure to chemicals or electromagnetic stress (Farci et al. 2023a). These properties come as no surprise when one considers the meticulously structured nature of this cell envelope and the elaborate complexes re-

sponsible for its organization (Farci et al. 2021, 2022b). In fact, not limitedly to the S-layer, this cell envelope is a product of a precise tiling of a recurring unit, hereinafter referred to as the structural unit (SU), that covers in surface and thickness the entire cell envelope (Farci et al. 2021, 2022b). This recurring unit comprises three distinct complexes: the S-layer deinoxanthin binding complex (SDBC), a type II secretion system (T2SS), and an uncharacterized radial complex (RC) (Farci et al. 2022b; Farci and Piano 2023). Within the unit, a single T2SS orchestrates six SDBCs through lateral interactions, together with six RCs anchored on the outer membrane. The RC is most likely linked to the protruding extension of the hexagonal packing intermediate (HPI) located mainly on the uppermost layer (Bharat et al. 2023; von Kügelgen et al. 2023) and for which the main body, carrying the pore region, was glimpsed in previous cryo-EC works (Farci et al. 2022b; Farci and Piano 2023). This distinctive arrangement, distinguished by its characteristic p6 symmetry, contributes to an assembly exceeding 6 MDa.

Noteworthy, further cohesion to the SU is provided by the SDBC through the subunit DR_2577 (or SlpA), which exhibits a peculiar arrangement of its S-layer Homology (SLH) domain, a not-exclusively characteristic of S-layer proteins (Beveridge et al. 1997; Mesnage et al. 2000; Sleytr et al. 2014), tethered towards the inner membrane.

In addition to this remarkable complexity is the observation that the systematic repetition results in a structure exhibiting paracrystalline traits, as evidenced by its diffractive attributes (Farci et al. 2021, 2022b). This offers an additional clue to the intriguing specialization at play. When it comes to functionality, as per our current understanding, the SDBC stands out as the primary complex accountable for the protective properties in this cell envelope (Farci et al. 2016, 2018, 2019, 2020, 2021, 2022a, 2023a). Nevertheless, it is important to acknowledge the potential coexistence of additional supplementary or alternative protective mechanisms that could also serve crucial roles. Although the functional rationale behind this remarkable specialization remains uncertain, particularly considering the substantial expenditure of mass and energy it entails, the existence of such a condensed arrangement prompts a deeper consideration. How much free space exists within this densely packed organization? How are the remaining vital machineries distributed across the periplasm, the inner and outer membranes? Considering the literature produced so far, here we address these inquiries by employing a dimensional analysis of the atomic structures inherent to the three primary complexes (SDBC, T2SS, and HPI) and their respective positioning within the cell envelope. As it will be shown here, despite the tightly packed nature of the structure, the complexes also show a large amount of unoccupied space. In fact, this tight packing has also local variations in density between the layers of the cell envelope. Similar to the arrangement of threads in fabric, the interaction between complexes exhibits a pattern of vertical warp and horizontal weft. However, in contrast to textiles, these complexes do not display equivalent levels of interlacement, showing a reduced degree of density vertically and a heightened level horizontally. Consequently, this characteristic results into less vertical density especially in the

large periplasmic space, hence, within the membrane layers. This distinction is particularly pronounced in the outer membrane and less for the inner membrane that appears less populated by the components of the SU.

Results are examined while considering crucial factors such as the notable absence of many uncharacterized complexes/proteins (e.g., the RC, the uncharacterized SDBC and T2SS subunits, and many other proteins frequently with unknown function and typical of this cell envelope—Farci et al. 2014) and the presence of an extended fraction of unoccupied space that could also host important cellular machineries (e.g., free enzymes taking care of homeostatic functions) not part of the regular packing. Additionally, concerning the key subunit of the SDBC, the protein DR_2577 (or SlpA) exhibits a peculiar arrangement with its SLH domain tethered towards the inner membrane rather than the outer, a not-exclusively characteristic of S-layer proteins that also binds to secondary cell wall polymers (Beveridge et al. 1997; Mesnage et al. 2000; Sleytr et al. 2014). These elements collectively contribute to increasing the complexity of this cell envelope, making even more challenging the understanding of its structural and functional network.

The presented findings and the information gleaned from recent reports are combined to create a comprehensive perspective. The functional implications of these findings are then explored in relation to the evolutionary pressures of various environmental surface phenomena that might have been affecting the cell envelope shaping it as appears today.

Materials and methods

Visualization and models fitting

The cryo-EM maps either of the cell envelope patch or the complexes, as well as the pdb model of the complexes, were visualized using the Chimera software (Pettersen et al. 2004). As a first step each complex (map and pdb) was inserted into the 3D cryo-electron crystallography (cryo-EC) map of the cell envelope (Farci et al. 2022b) using the “Fit in map” tool and subsequently manually adjusted. For the SDBC, after fitting the first copy, the remaining five were placed by rotating of 60°, 120°, 180°, 240°, and 300°, respectively, keeping the same relative orientation with respect to the center of the T2SS. The HPI in its hexameric form was obtained fitting six copies of the monomer into the single-particle cryo-EM map and oriented according to von Kügelgen et al. (2023) before inserting it into the cryo-EC map (Farci et al. 2022b). Furthermore, a more precise alignment on-plane was performed by superposing the 2D cryo-EC map (Farci et al. 2021) as a higher resolution reference for the top view. The obtained final fitting allowed to visualize the complete model of the SU.

Calculation of macromolecular volumes and surfaces

The 3V web server (Voss and Gerstein 2010; <http://3vee.molmovdb.org>) was used to calculate volumes, surface areas, and internal volumes with biological significance for all the complexes and for the resulting SU. As input information, the pdb models were provided to the web server.

In detail, we used four of the tools available in the 3V web server of which two were for calculating the external volumes and two for the internal ones.

External volumes calculations

As a first step, the external volumes at different probe radius were calculated. Particularly, to have a good approximation of the volumes occupied by the whole atoms in the complex, the Van der Waals volume and related surface were calculated. To this aim, the Volume Assessor tool at a probe radius 0 Å was applied. Subsequently, the volume was extended first to the regions not accessible to solvent and then to this volume was also included the one occupied by the solvent (water). For this aim, the Volume Probe Range tool was applied with a minimum and a maximum probe radius of 1.4 and 2.4 Å, respectively, at a step of 1 Å. This allowed to obtain the volume (and related surface) of a given complex including the regions not accessible to solvent (1.4 Å) and the total volume inclusive of the regions accessible to solvent (2.4 Å). These measurements were done for the whole complexes.

Internal volumes calculations

From the obtained external volumes, the internal volumes were finally extracted. As a first step, the volume of the solvent was extracted by applying the Solvent Extractor tool at 3.5 and 12.0 Å as an inner and an outer probe radius, respectively. In these conditions were obtained the shell and the solvent-excluded volumes from which, by subtracting one from the other, the final internal volume (and related surfaces) is calculated. Finally, to identify internal volume fractions ascribable to pores, channels, cavities and clefts, the Channel Finder tool was applied. Here, the parameters used for the previous tool were maintained for SDBC and HPI, while for the T2SS 20.0 and 50.0 Å were applied as an inner and an outer probe radius, respectively. A cutoff of maximum nine channels was applied for all the complexes analyzed.

Results

Docking studies reveal an extended juxtaposition within and between the cell envelope units

The organization of the major cell envelope complexes, the SDBC, the T2SS, and the RC, within *D. radiodurans* has been unveiled at middle–low resolutions through 2D and 3D cryo-EM maps obtained by cryo-electron crystallography (cryo-EC; Farci et al. 2021, 2022b; Farci and Piano 2023). These structural analyses provided valuable insights into the relative localization among the three complexes and hints about their spatial relationships. Additionally, for a part of the major complexes structural information became available in the last few years. In fact, atomic resolution structures provided great details for the SDBC (von Kügelgen et al. 2022; Farci et al. 2022a, 2023a) and the T2SS (Farci et al. 2023b). Notably,

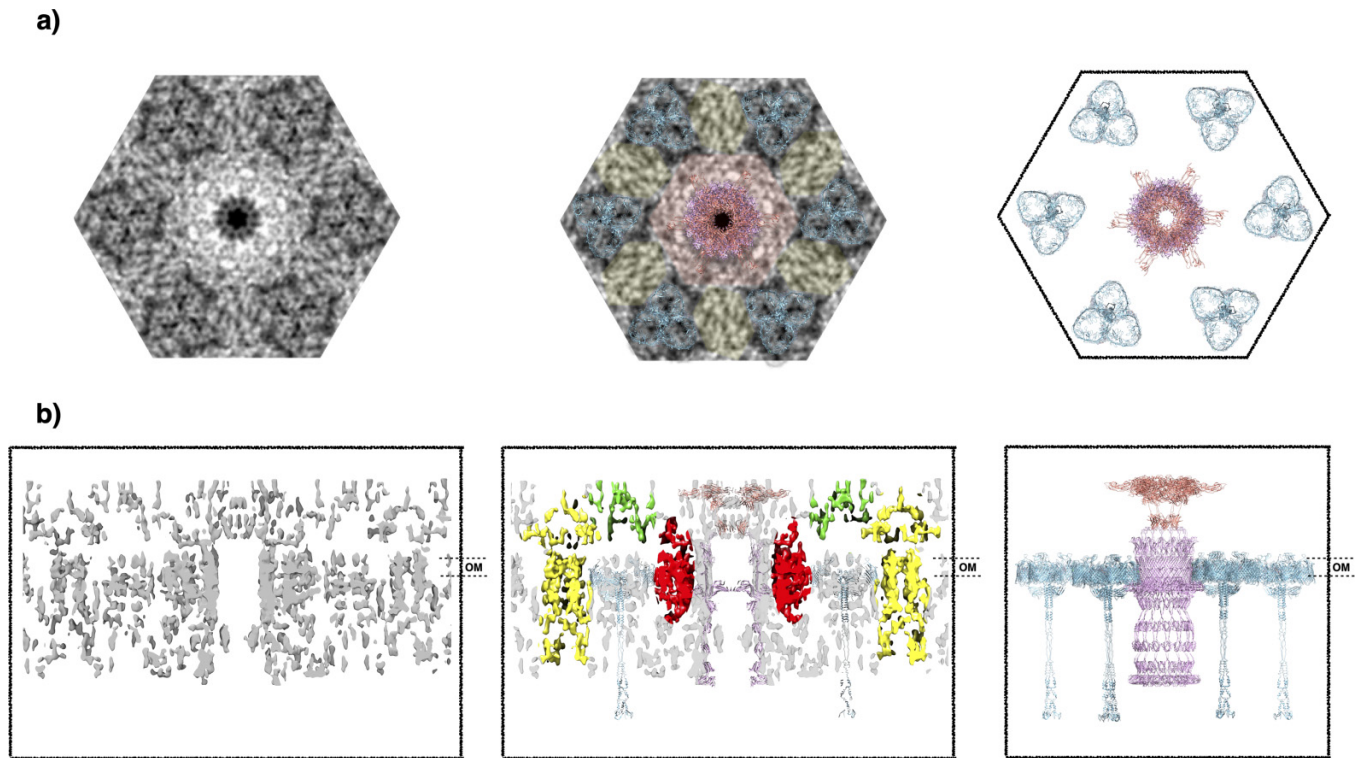
an atomic resolution structure for the HPI of the protein DR_2508 (von Kügelgen et al. 2023), likely connected to the RC complex (RC-HPI), has also been published. Finally, a low-resolution structure is available for the outer membrane region of the RC, the Radial-Dimer Complex (Farci et al. 2022b).

In an effort to understand the degree of apparent versus actual density/rigidity within this cell envelope, we gathered the information from the abovementioned structural achievements, as schematically shown in Fig. 1. We therefore integrated the available atomic resolution models for SDBC, T2SS, and HPI, into the 2D and 3D cell envelope maps obtained by cryo-EC, with the orientation into the cell envelope done according to Farci et al. (2023a, 2023b) for SDBC and T2SS, and to von Kügelgen et al. (2023) for HPI. The spatial organization of this cell envelope has been previously shown by cryo-electron tomography studies further processed with a subtomogram averaging or cryo-electron crystallography approach, either imposing or not a p6 symmetry (Farci et al. 2021, 2022b, 2023b). This allowed modeling a structural unit comprising one T2SS, six SDBC, and one HPI positioned atop (Fig. 1a), revealing a precise relative positioning of these complexes. Furthermore, aside from aiding in understanding the spatial organization of the three cell envelope complexes, this approach revealed other relevant details. In particular, the identification of a component positioned atop the SDBC (green region in Fig. 1b), the connection between the HPI and the RC (red and yellow regions in Figs. 1a and 1b), an alignment of the HPI with the T2SS pore through its channel region (T2SS-HPI; Figs. 1a and 1b), and an extension of the RC from the outer membrane into the S-layer and the periplasm (yellow region in Fig. 1b).

Exploring the extent of pores, channels, clefts, and cavities within the cell envelope complexes

Having clarified the relative position of the components within the structural unit responsible for the regularity of this cell envelope, our focus shifted to assessing the unoccupied space within this unit. We systematically identified these areas and proceeded to analyze their distribution patterns. This particular information holds significance as it pertains to the occurrence of crucial cell functions and related machineries (Han et al. 2020) that do not conform to the regular packing arrangement. To achieve this objective, we initially characterized the unoccupied space inherent to each complex holding functional and/or structural significance. In this regard, we performed the following volumes assessments, according to the definitions of Voss and Gerstein (2010): (i) measurement of the three pores within the SDBC complex; (ii) determination of the uninterrupted channel continuity between the T2SS and RC-HPI complexes as well as less evident channels in the complexes; and (iii) identification of internal protein volumes as clefts and cavities. The former two, pores and channels, are identified as functional regions within a given complex of the SU as emerged from their functional and structural characterization, whereas the latter, clefts, and cavities, are defined as structural void within a given complex of the SU and distinguished on the base of their volumetric extension. Accordingly, this portion of space

Fig. 1. Model of the structural unit based on the cryo-EC maps. The image presents a schematic representation as top view (a) and side view (b) of the main structural unit of this cell envelope. In (a), the image shows the 2D cryo-EC map of the minimal repeating unit as obtained from the unit cell after processing (upper left); in the same map the different regions are indicated with colors: in light blue the S-layer deinoxanthin binding complex atomic resolution model; in two different shades of pink the atomic resolution models of hexagonal packing intermediate and type II secretion system; in yellow the radial complex; in red the regions surrounding the T2SS linked to the RC and the SDBC (upper central); the structural unit with only the atomic resolution models is also shown (upper right). In (b), the 3D cryo-EC map shows a side view of the unit cell with a cross section at the center of the T2SS cutting the main diagonal of the unit cell (bottom left); the same map shows the fitting of SDBC (light blue), HPI and T2SS (shades of pink), and the low-resolution densities of the RC (yellow) and other unassigned complexes (green and red) (bottom center). Finally, a model reporting the only atomic resolution structures for SDBC, T2SS, and HPI is also shown (bottom right).



is essential for allowing both the structural and functional presence of a given complex.

For each of the three complexes, we initially calculated the Van der Waals volume (and related surface) assuming it to be a good approximation of the volumes occupied by the whole atoms in the complex. Then, we extended this calculation including the volume within the protein structure that is not accessible to the solvent (water), and finally further extended this volume to the spaces typically accessible to water, here referred to as the internal volume (IV). By this approach, for each complex it was possible to obtain three different volumes and related surfaces as such (i) the Van der Waals volume and surface, V_{vw} and S_{vw} , respectively; (ii) the solvent-excluded volume and surface, V_{se} and S_{se} , respectively; and (iii) the solvent-included volume and surface, V_{si} and S_{si} , respectively (Table 1). The obtained volumes and surfaces were processed as reported by Voss and Gerstein (2010), allowing to obtain the total net volume (and related surface) of solvent and further separate it in functional fractions related with pores and channel and structural

fractions related with clefts, cavities, and residual secondary portions (Table 2). In detail, the SDBC is the only complex having multiple pores, which are three for each complex and account for $\sim 9.1 \times 10^4 \text{ \AA}^3$ ($\sim 68\%$ of the IV for this complex) (Fig. 2a). Interestingly, for this complex also several channel regions were identified ($\sim 1.3 \times 10^4 \text{ \AA}^3$; $\sim 9.9\%$ of the IV for this complex). In particular, it is worth of mention an extended region separated in two parts and localized at the base of the stalk as also other regions of the coiled coil, suggesting it to likely be a single long channel (Fig. 2a). The T2SS was found to be composed of a channel, accounting for $\sim 4.4 \times 10^5 \text{ \AA}^3$ ($\sim 31\%$ of the IV for this complex), and a pore, accounting for $\sim 9.9 \times 10^5 \text{ \AA}^3$ ($\sim 69\%$ of the IV for this complex). Importantly, the top part of the T2SS channel is in continuity with the only one channel found in the RC-HPI, which accounts for $\sim 3.5 \times 10^4 \text{ \AA}^3$ ($\sim 30\%$ of the IV for this complex) (Fig. 2b). The rest of the IV for both these complexes is fragmented and accounts for small clefts, cavities, and residual holes that are of structural relevance rather than functional one.

Table 1. Volumes and surfaces of the cell envelope complexes in different conditions.

Complex	Protein volume (V) (Å ³)			Protein surface (S) (Å ²)			Volume/surface (V/S)		
	V _{vw} [*]	V _{se} [†]	V _{si} [‡]	S _{vw} [*]	S _{se} [†]	S _{si} [‡]	V _{vw} /S _{vw}	V _{se} /S _{se}	V _{si} /S _{si}
SDBC	340 671	538 925	533 775	296 563	145 438	122 715	1.15	3.70	4.35
T2SS	1 230 367	1 989 505	2 008 765	1 099 082	492 678	387 510	1.12	4.04	5.18
HPI	522 815	827 643	830 536	457 872	166 310	130 930	1.14	4.98	6.34

Note: The differences are highlighted by ratios between volume and surface.

^{*}Van der Waals volume (V_{vw}) and surface (S_{vw}).

[†]Solvent-excluded volume (V_{se}) and surface (S_{se}).

[‡]Solvent-included volume (V_{si}) and surface (S_{si}).

Table 2. Internal volumes and surfaces of the cell envelope complexes.

Complex	Internal volume (IV) (Å ³)				Internal surface (IS) (Å ²)				Total IV/IS
	Pores	Channels	Clefts and residual cavities	Total IV	Pores	Channels	Clefts and residual cavities	Total IS	
SDBC	91 317	13 259	29 264	133 840	32 994	5879	19 409	58 282	2.3
T2SS	995 661	442 250	0	1437 911	57 286	31 800	0	89 086	16.1
HPI	0	35 330	82 292	117 622	0	13 140	51 157	64 297	1.83

Note: Cavities are also assigned on the base of their shapes and dimensions.

To this analysis must be taken into account the remaining part consisting of both the free space at the interface between complexes and the occupied space related to the so-far uncharacterized complexes also part of the SU (Fig. 1b).

Exploring the heterogeneous density in the cell envelope complexes architecture reveals extended free space regions

In the concluding part of our investigation, we quantified the complete extent of unoccupied space within each structural unit, and, from this value, we subtracted the portion attributed to the functional and structural free space within each complex. With respect to each other, when calculated its hindrance volume (V_h; surface of the complex × its height) the defined SU encompassed a volume of $\sim 1.63 \times 10^8$ Å³, with individual contributions from the SDBC, T2SS, and HPI complexes, calculated in a similar way, amounting to $\sim 3.53 \times 10^6$, $\sim 7.82 \times 10^6$, and $\sim 2.86 \times 10^6$ Å³, respectively (Table 3). Notably, the observation that the overall SU volume exceeds approximately 11.5 times the combined volume of its individual components (when summed, the value of V_h of the individual components accounts for a mere 8.7% of the unit's volume) provides a crucial indication that a considerable portion of the volume could potentially be unoccupied space within the SU or occupied by other integral SU complexes for which structural information is still missing, as shown in Fig. 1b by the presence of low-resolution densities in the 3D cryo-EC map. Moreover, the former should be intended as free space as well as space occupied by machineries that are not part of the ordered packing of this cell envelope.

This observation becomes even more significant when taking the V_{si} sum of the three complexes with respect to the V_h of the SU ($\sim 2.1\%$).

This analysis revealed that an extended fraction of the structural unit is composed of unoccupied space. Importantly, this identical percentage can be extrapolated to en-

compass the entire cell envelope. As a result of this analysis, it becomes evident that within its density, the cell envelope contains a notable volume of space that can accommodate various machineries and their crucial cellular functions.

Discussion

The surface density of the cell envelope in *Deinococcus radiodurans* has been recently elucidated using cryo-EC (Farci et al. 2021; 2022b). Recent studies have shown how this tightly organized structure plays a pivotal role in effectively managing nutrient transport and providing protection against detrimental chemical and physical influences (Farci et al. 2016, 2018, 2021, 2022a, 2023a). However, in the same studies, as well as in investigations focused on individual components of the SU (Farci et al. 2022a, 2023a, 2023b; von Kügelgen et al. 2023), it appears evident how the degree of surface density is likely to fluctuate throughout the thickness of the cell envelope and its SU. Here, this variation was thoroughly investigated, revealing a notable portion of the cell envelope to be composed of “empty space”, especially in the layers below the outer membrane. This space might refer to either vacant areas or volumes occupied by proteins not part of the regular packing, thus not contributing to the diffraction properties typical of this cell envelope. This observation holds great significance due to the functional and structural nature of this cell envelope organization. In fact, this part of the cell is intrinsically linked to two critical factors: firstly, the requirement for volumes that can accommodate essential machineries crucial for cellular function but not part of the SU itself (Han et al. 2020), and secondly, the necessity for a densely packed surface configuration that couples protective properties with a rational trafficking of nutrients (Farci et al. 2022a, 2023a). All these aspects conspicuously contrast with each other, with the thickness primarily required to accommodate “low-density” volumes (to provide available spaces for crucial machineries), while conversely, the surface oppositely

Fig. 2. Localization of pores and channels in the main cell envelope complexes. According to the so-far-known protein composition of the structural unit of this cell envelope, a schematic representation of the internal volumes of each protein complexes is shown. In (a), the upper figure shows a top view of the S-layer deinoxanthin binding complex model detailing the three pores (yellow-to-orange) and the central channel (dark pink). The bottom figure shows a side view of the SDBC evidencing the pore region (yellow-to-orange) and a discontinuous central channel (dark pink). In (b), it is shown a top view of the hexagonal packing intermediate-type II secretion system assembly with a detail of the central channel depicted in white-to-red (left), while on the right is shown a side view of the same assembly evidencing the extended channel region involving the HPI and the upper part of the T2SS (white-to-red) and the pore region involving the bottom part of the T2SS (yellow-to-orange).

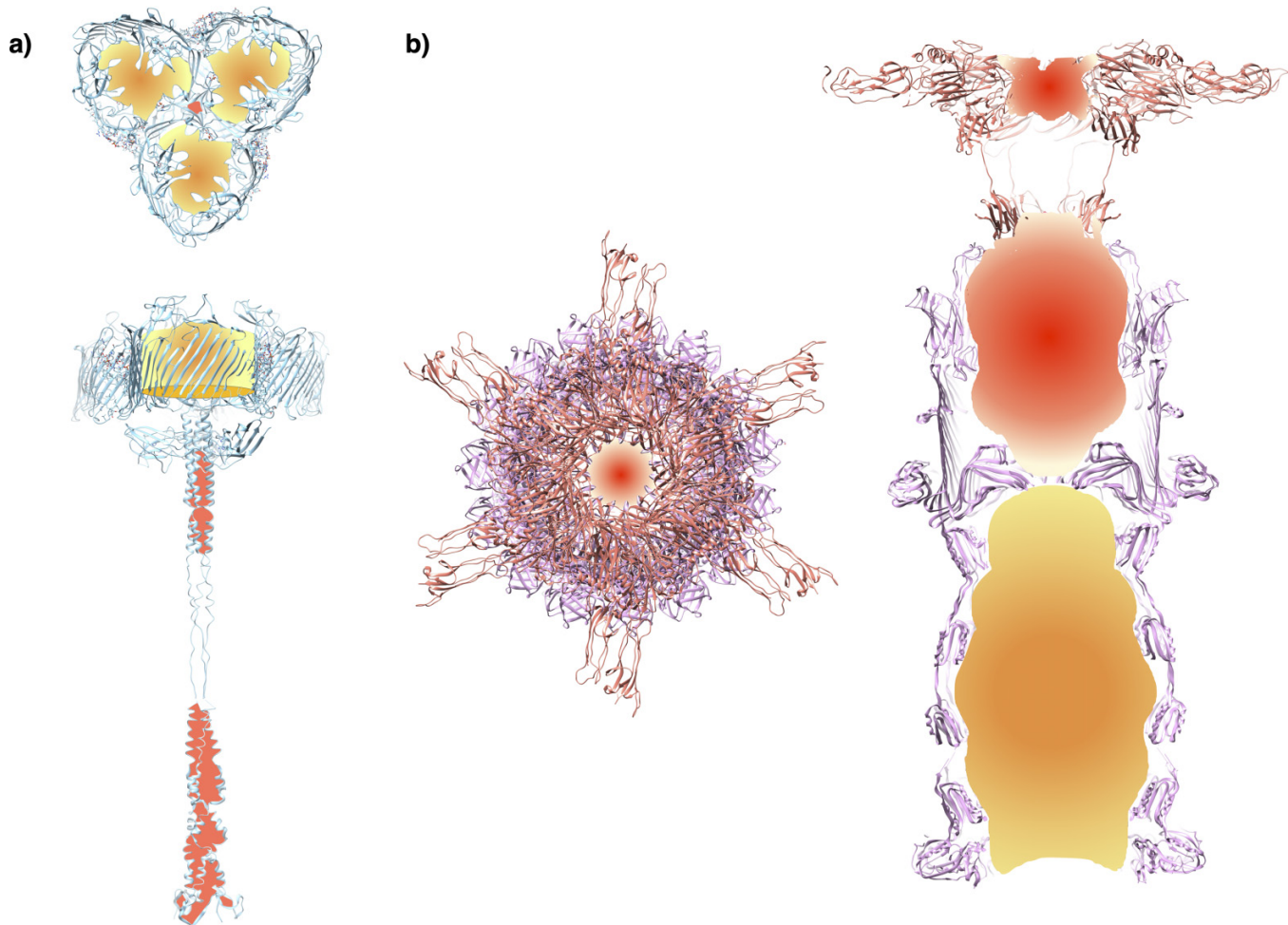


Table 3. Free external volumes around each cell envelope complex allowing other machineries' activities.

Complex	V_h^* (\AA^3)	V_{si}^\dagger (\AA^3)	IV^\ddagger (\AA^3)	$(V_h - V_{si})/V_{si}^\dagger$	$IV^\ddagger/V_{si}^\dagger$
SDBC	3 530 816	533 775	133 840	5.61	0.25
T2SS	7 829 250	2 008 765	1 437 911	2.90	0.72
HPI	2 862 522	830 536	117 622	2.45	0.14
Cell envelope unit	163 057 698	—	—	—	—

*The hindrance volume (V_h) obtained by multiplying the area of the top view of the particle, which serves as the base, by its corresponding height (102 64 × 344 for the SDBC; 237 25 × 330 for the T2SS; 244 66 × 117 for the HPI; 273 358 × 519 for the cell envelope unit).

†Solvent-included volume (V_{si}).

‡Internal volume (IV).

demands “high-density” (to allow protection and controlled trafficking). Significantly, this dimensional disparity (volume vs. surface) emerges as a key aspect for comprehending this intricate structure. On one hand, the volume consideration

stems from the necessity to house vital machineries and facilitate their functions. On the other hand, the surface imperative arises from the need to defend against factors predominantly manifesting on the surface due to environmental

pressures. In connection to this last aspect, it is important to recognize that the protective role can indeed be attributed also to the inherent surface density of this cell envelope. The protective functions associated with the cell envelope have been extensively documented, encompassing both preventive and reparative actions (Farci et al. 2016, 2018, 2021, 2022a, 2023a). Among the preventive roles, a noteworthy consideration involves energetic surface phenomena of environmental origin such as irradiation and electromagnetic stress. These factors lead to the emission of energy through heat and fluorescence, thereby impacting on the integrity of the cell envelope, which, as a result, is additionally tasked with mitigating the induced evaporation and desiccation events. This perspective sheds light on the remarkable resistance of *D. radiodurans* to electromagnetic stress, heat, and desiccation, further emphasizing the multifaceted protective mechanism inherent to this cell envelope. The particular resilience is exemplified by the heightened density/rigidity observed towards the upper section of the SU. This characteristic is underscored by the analysis presented, wherein the HPI (an exclusively surface complex) exhibits an increased V_{si}/S_{si} ratio in contrast to the T2SS and SDBC complexes (both extending in the cell envelope thickness) (Table 1). These latter ones are distinguished by a notably extended z-axis, influencing the overall sphericity of the complex including their V_{si}/S_{si} . Similar insights could be expected for the V_{si}/S_{si} ratios in the outer membrane regions of both SDBC and T2SS. These findings are reinforced by the uniformity observed in the V_{vw}/S_{vw} ratios across the complexes. Consistently, this particular ratio directly relates to the volume fraction that remains unaffected by interactions with the surrounding environment. An essential addition to this context is the uniform distribution of pores. Following irradiation and subsequent protection, the system experiences evaporation, leading to desiccation. This aspect holds significance due to the potential loss of surface water, which could trigger the movement of water from the cell's interior, accelerating desiccation. Conversely, drawing a parallel to the stomatal system in plant leaves, the presence of an impermeable surface punctuated by pores assumes a pivotal role in curtailing water loss. In this context, it is worth noting that, similar to stomata in plant leaves, there is a possibility within this S-layer that pores could exhibit the capability to transition from an open to a closed state, as indicated by previous findings (Müller et al. 1996).

This analysis highlights the interplay between the intricate organization and the resulting complex function of this cell envelope, which is closely intertwined with primary environmental pressures driven by electromagnetic energy, as well as the subsequent secondary environmental pressure focused on minimizing evaporation and desiccation. Naturally, these processes occur while upholding the fundamental operations of the cellular envelope. These dynamics underpin the development of a cell envelope characterized by a compact surface and a more relaxed thickness.

Based on the points discussed earlier, there are specific aspects related to the cell envelope of *D. radiodurans* that require further clarification. The abovementioned cell envelope studies did not focus on the septa, which contain only

the inner membrane and peptidoglycan (Rothfuss et al. 2006; Floc'h et al. 2018, 2019). Considering the architecture of *D. radiodurans* cell envelope is essential to understand how the septa are included into this organization. Accordingly, two alternative models can be envisaged. If the cell envelope exhibits a highly organized structure also in the inner membrane layer due to functional relationships with the outer membrane and S-layer complexes, it would be valuable to investigate whether any reorganization events occur during septa formation. Conversely, if the cell envelope lacks a highly organized structure in the inner membrane, it becomes interesting to explore whether a specific protein arrangement exists within the septa, where a regular arrangement might facilitate the exchange between cells of the same tetrad.

In conclusion, summarizing the structural and functional information provided by the existing literature (Daly et al. 2007; Farci et al. 2016, 2018, 2021, 2022a, 2023, 2023b; Yu et al. 2017; Santos et al. 2019; von Kügelgen et al. 2023) and the novel insight gleaned from this study, the cell envelope of *D. radiodurans* appears to serve as a remarkably organized and “functionalized” protective organelle. The intricate structure mediated by specialized multi-subunit protein complexes contributes to provide this extremophile bacterium with an exceptional resistance to extreme conditions while maintaining integrity and basic cellular functions. Eventually, the insights here provided might tickle further exploration of the mechanisms underlying the envelope's functions to unveil additional information into the evolution and remarkable adaptability of *D. radiodurans* survival strategies.

Acknowledgements

This work was supported by the National Science Center (Poland) with the Sonata BIS 7 Program (2017) Grant PRO-2017/26/E/NZ1/00344 and the Harmonia 10 Program (2018) Grant PRO-2018/30/M/NZ1/00284 (both to DP and DF).

Article information

History dates

Received: 22 September 2023

Revised: 17 January 2024

Accepted: 30 January 2024

Version of record online: 25 March 2024

Notes

This paper is a part of the tribute collection entitled “Dr. Robert Murray: Strong roots in Canadian microbiology - Strong global leadership and vision.” <https://cdnsiencepub.com/topic/cjm-murray-tribute>.

Copyright

© 2024 The Author(s). This work is licensed under a [Creative Commons Attribution 4.0 International License](https://creativecommons.org/licenses/by/4.0/) (CC BY 4.0), which permits unrestricted use, distribution, and reproduction in any medium, provided the original author(s) and source are credited.

Data availability

Materials, data, and associated protocols are available within the manuscript and the public repository Electron Microscopy Data Bank (EMDB; <https://www.ebi.ac.uk/emdb/>). Cell envelope 3D map accession code: EMD-14097; T2SS accession codes EMD-16770 and PDB ID-8CO1; SDBC accession codes: EMD-15487, EMD-15382, EMD-15384, PDB-8ACQ, and PDB-8AGD; HPI accession codes: EMD-16694 and PDB-8CKA (assembly 1).

Author information

Author ORCIDs

Domenica Farci <https://orcid.org/0000-0002-3691-2699>

Dario Piano <https://orcid.org/0000-0003-2980-7572>

Author contributions

Conceptualization: DF, DP

Data curation: DF, DP

Formal analysis: DF, DP

Funding acquisition: DF, DP

Investigation: DF, DP

Methodology: DF, DP

Project administration: DF, DP

Resources: DF, DP

Supervision: DF, DP

Validation: DF, DP

Visualization: DF, DP

Writing – original draft: DF, DP

Writing – review & editing: DF, DP

Competing interests

The authors declare that they have no competing interests.

References

- Anderson, A., Nordan, H., Cain, R., Parrish, G., and Duggan, D. 1956. Studies on a radioresistant micrococcus. I. Isolation, morphology, cultural characteristics, and resistance to gamma radiation. *Food Technol.* **10**: 575–578.
- Anderson, R., and Hansen, K. 1985. Structure of a novel phosphoglycolipid from *Deinococcus radiodurans*. *J. Biol. Chem.* **260**: 12219–12223. doi:10.1016/S0021-9258(17)39012-9. PMID: 4044593.
- Beveridge, T.J., Pouwels, P.H., Sára, M., Kotiranta, A., Lounatmaa, K., Kari, K., et al. 1997. Functions of S-layers. *FEMS Microbiol. Rev.* **20**(1–2): 99–149. doi:10.1111/j.1574-6976.1997.tb00305.x. PMID: 9276929.
- Bharat, T.A.M., Tocheva, E.I., and Alva, V. 2023. The cell envelope architecture of *Deinococcus*: HPI forms the S-layer and SlpA tethers the outer membrane to peptidoglycan. *Proc. Natl. Acad. Sci. U.S.A.* **120**(51): e2305338120. doi:10.1073/pnas.2305338120. PMID: 38085775.
- Brooks, B.W., and Murray, R.G.E. 1981. Nomenclature for “*Micrococcus radiodurans*” and other radiation-resistant cocci: *Deinococcaceae* fam. nov. and *Deinococcus* gen. nov., including five species. *Int. J. Syst. Bacteriol.* **31**: 353–360. doi:10.1099/00207713-31-3-353.
- Cox, M.M., and Battista, J.R. 2005. *Deinococcus radiodurans*—the consummate survivor. *Nat. Rev. Microbiol.* **3**(11): 882–892. doi:10.1038/nrmicro1264. PMID: 16261171.
- Daly, M.J. 2023. The scientific revolution that unraveled the astonishing DNA repair capacity of the *Deinococcaceae*: 40 years on. *Can. J. Microbiol.* doi:10.1139/cjm-2023-0059.
- Daly, M.J., Gaidamakova, E.K., Matrosova, V.Y., Vasilenko, A., Zhai, M., Leapman, R.D., et al. 2007. Protein oxidation implicated as the primary determinant of bacterial radioresistance. *PLoS Biol.* **5**(4): e92. doi:10.1371/journal.pbio.0050092. PMID: 17373858.
- Daly, M.J., Gaidamakova, E.K., Matrosova, V.Y., Vasilenko, A., Zhai, M., Venkateswaran, A., et al. 2004. Accumulation of Mn (II) in *Deinococcus radiodurans* facilitates gamma-radiation resistance. *Science*, **306**(5698): 1025–1028. doi:10.1126/science.1103185. PMID: 15459345.
- Farci, D., and Piano, D. 2023. Reply to Bharat et al.: continuity or discontinuity, that is the question. *Proc. Natl. Acad. Sci. U.S.A.* **120**(51): e2311568120. doi:10.1073/pnas.2311568120. PMID: 38085786.
- Farci, D., Bowler, M.W., Kirkpatrick, J., McSweeney, S., Tramontano, E., and Piano, D. 2014. New features of the cell wall of the radio-resistant bacterium *Deinococcus radiodurans*. *Biochim Biophys Acta*, **1838**(7): 1978–84. doi:10.1016/j.bbamem.2014.02.014.
- Farci, D., Slavov, C., Tramontano, E., and Piano, D. 2016. The S-layer Protein DR_2577 Binds Deinoxanthin and under Desiccation Conditions Protects against UV-Radiation in *Deinococcus radiodurans*. *Front Microbiol.*, **7**: 155. doi:10.3389/fmicb.2016.00155.
- Farci, D., Slavov, C., and Piano, D. 2018. Coexisting properties of thermostability and ultraviolet radiation resistance in the main S-layer complex of *Deinococcus radiodurans*. *Photochem Photobiol Sci.*, **17**(1): 81–88. doi:10.1039/c7pp00240h.
- Farci, D., Guadalupi, G., Bierła, K., Lobinski, R., and Piano, D. 2019. The Role of Iron and Copper on the Oligomerization Dynamics of DR_2577, the Main S-Layer Protein of *Deinococcus radiodurans*. *Front Microbiol.*, **10**: 1450. doi:10.3389/fmicb.2019.01450.
- Farci, D., Aksoyoglu, M.A., Farci, S.F., Bafna, J.A., Bodrenko, I., Ceccarelli, M., et al. 2020. Structural insights into the main S-layer unit of *Deinococcus radiodurans* reveal a massive protein complex with porin-like features. *J Biol Chem.*, **295**(13): 4224–4236. doi:10.1074/jbc.RA119.012174.
- Farci, D., Kereiche, S., Pangei, S., Haniewicz, P., Bodrenko, I.V., Ceccarelli, M., et al. 2021. Structural analysis of the architecture and in situ localization of the main S-layer complex in *Deinococcus radiodurans*. *Structure*, **29**(11): 1279–1285.e3. doi:10.1016/j.str.2021.06.014. PMID: 34265277.
- Farci, D., Haniewicz, P., de Sanctis, D., Iesu, L., Kereiche, S., Winterhalter, M., and Piano, D. 2022a. The cryo-EM structure of the S-layer deinoxanthin-binding complex of *Deinococcus radiodurans* informs properties of its environmental interactions. *J. Biol. Chem.* **298**(6): 102031. doi:10.1016/j.jbc.2022.102031. PMID: 35577074.
- Farci, D., Haniewicz, P., and Piano, D. 2022b. The structured organization of *Deinococcus radiodurans*’ cell envelope. *Proc. Natl. Acad. Sci. U. S. A.* **119**(45): e2209111119. doi:10.1073/pnas.2209111119. PMID: 36322746.
- Farci, D., Graça, A.T., Iesu, L., de Sanctis, D., and Piano, D. 2023a. The SDBC is active in quenching oxidative conditions and bridges the cell envelope layers in *Deinococcus radiodurans*. *J. Biol. Chem.* **299**(1): 102784. doi:10.1016/j.jbc.2022.102784. PMID: 36502921.
- Farci, D., Milenkovic, S., Iesu, L., Tanas, M., Ceccarelli, M., and Piano, D. 2023b. Structural characterization and functional insight into the type II secretion system of the poly-extremophile *Deinococcus radiodurans*. *J. Biol. Chem.* **8**: 105537. doi:10.1016/j.jbc.2023.105537.
- Floc’h, K., Lacroix, F., Barbieri, L., Servant, P., Galland, R., Butler, C., et al. 2018. Bacterial cell wall nanoimaging by autoblinking microscopy. *Sci. Rep.* **8**(1): 14038. doi:10.1038/s41598-018-32335-z. PMID: 30232348.
- Floc’h, K., Lacroix, F., Servant, P., Wong, Y.S., Kleman, J.P., Bourgeois, D., and Timmins, J. 2019. Cell morphology and nucleoid dynamics in dividing *Deinococcus radiodurans*. *Nat. Commun.* **10**(1): 3815. doi:10.1038/s41467-019-11725-5. PMID: 31444361.
- Han, R., Fang, J., Jiang, J., Gaidamakova, E.K., Tkavc, R., Daly, M.J., and Contreras, L.M. 2020. Signal recognition particle RNA contributes to oxidative stress response in *Deinococcus radiodurans* by modulating catalase localization. *Front. Microbiol.* **11**: 613571. doi:10.3389/fmicb.2020.613571. PMID: 33391243.
- Huang, Y., and Anderson, R. 1989. Structure of a novel glucosamine-containing phosphoglycolipid from *Deinococcus radiodurans*. *J. Biol. Chem.* **264**: 18667–18672. doi:10.1016/S0021-9258(18)51519-2. PMID: 2808391.
- Huang, Y., and Anderson, R. 1991. Phosphatidylglyceroylalkylamine, a novel phosphoglycolipid precursor in *Deinococcus radiodurans*. *J.*

- Bacteriol. **173**: 457–462. doi:10.1128/jb.173.2.457-462.1991. PMID: 1987140.
- Huang, Y., and Anderson, R. 1995. Glucosyl diglyceride lipid structures in *Deinococcus radiodurans*. J. Bacteriol. **177**: 2567–2571. doi:10.1128/jb.177.9.2567-2571.1995. PMID: 7730293.
- Ji, H.F. 2010. Insight into the strong antioxidant activity of deinoxanthin, a unique carotenoid in *Deinococcus radiodurans*. Int. J. Mol. Sci. **11**: 4506–4510. doi:10.3390/ijms11114506. PMID: 21151452.
- Lemeë, L., Peuchant, E., Clerc, M., Brunner, M., and Pfander, H. 1997. Deinoxanthin: a new carotenoid isolated from *Deinococcus radiodurans*. Tetrahedron, **53**(3): 919–926. doi:10.1016/S0040-4020(96)01036-8.
- Mesnager, S., Fontaine, T., Mignot, T., Delepierre, M., Mock, M., and Fouet, A. 2000. Bacterial SLH domain proteins are non-covalently anchored to the cell surface via a conserved mechanism involving wall polysaccharide pyruvylation. EMBO J. **19**(17): 4473–4484. doi:10.1093/emboj/19.17.4473. PMID: 10970841.
- Müller, D.J., Baumeister, W., and Engel, A. 1996. Conformational change of the hexagonally packed intermediate layer of *Deinococcus radiodurans* monitored by atomic force microscopy. J. Bacteriol. **178**(11): 3025–3030. doi:10.1128/jb.178.11.3025-3030.1996. PMID: 8655475.
- Murray, R.G., Hall, M., and Thompson, B.G. 1983. Cell division in *Deinococcus radiodurans* and a method for displaying septa. Can. J. Microbiol. **29**(10): 1412–1423. doi:10.1139/m83-217. PMID: 6661703.
- Murray, R.G.E. 1992. The family *Deinococcaceae*. In The prokaryotes. Edited by A. Balows, H.G. Trüper, M. Dworkin, W. Harder and K.H. Schleifer. Springer, New York, NY.
- Oshima, T., and Imahori, K. Description of *Thermus thermophilus* (Yoshida and Oshima) comb. Nov., a nonsporulating thermophilic bacterium from a Japanese Thermal Spa. Int. J. Syst. Evol. Microbiol. **24**(1974): 102–112.
- Ott, E., Kawaguchi, Y., Özgen, N., Yamagishi, A., Rabbow, E., Rettberg, P., et al. 2019. Proteomic and metabolomic profiling of *Deinococcus radiodurans* recovering after exposure to simulated low Earth orbit vacuum conditions. Front. Microbiol. **10**: 909. doi:10.3389/fmicb.2019.00909. PMID: 31110498.
- Pettersen, E.F., Goddard, T.D., Huang, C.C., Couch, G.S., Greenblatt, D.M., Meng, E.C., and Ferrin, T.E. 2004. UCSF Chimera—a visualization system for exploratory research and analysis. J. Comput. Chem. **25**: 1605–1612. doi:10.1002/jcc.20084. PMID: 15264254.
- Rothfuss, H., Lara, J.C., Schmid, A.K., and Lidstrom, M.E. 2006. Involvement of the S-layer proteins Hpi and SlpA in the maintenance of cell envelope integrity in *Deinococcus radiodurans* R1. Microbiology (Reading), **152**(Pt 9): 2779–2787. doi:10.1099/mic.0.28971-0.
- Santos, S.P., Yang, Y., Rosa, M.T.G., Rodrigues, M.A.A., De La Tour, C.B., Sommer, S., et al. 2019. The interplay between Mn and Fe in *Deinococcus radiodurans* triggers cellular protection during paraquat-induced oxidative stress. Sci. Rep. **9**(1): 17217. doi:10.1038/s41598-019-53140-2. PMID: 31748604.
- Sleytr, U.B., Schuster, B., Egelseer, E.M., and Pum, D. 2014. S-layers: principles and applications. FEMS Microbiol. Rev. **38**(5): 823–864. doi:10.1111/1574-6976.12063. PMID: 24483139.
- Tian, B., and Hua, Y. 2010. Carotenoid biosynthesis in extremophilic *Deinococcus-Thermus* bacteria. Trends Microbiol. **18**: 512–520. doi:10.1016/j.tim.2010.07.007. PMID: 20832321.
- Tian, B., Sun, Z., Shen, S., Wang, H., Jiao, J., Wang, L., et al. 2009. Effects of carotenoids from *Deinococcus radiodurans* on protein oxidation. Lett. Appl. Microbiol. **49**: 689–694. doi:10.1111/j.1472-765X.2009.02727.x. PMID: 19780959.
- Tian, B., Xu, Z., Sun, Z., Lin, J., and Hua, Y. 2007. Evaluation of the antioxidant effects of carotenoids from *Deinococcus radiodurans* through targeted mutagenesis, chemiluminescence, and DNA damage analyses. Biochim. Biophys. Acta, **1770**: 902–911. doi:10.1016/j.bbagen.2007.01.016. PMID: 17368731.
- von Kügelgen, A., van Dorst, S., Alva, V., and Bharat, T.A.M. 2022. A multidomain connector links the outer membrane and cell wall in phylogenetically deep-branching bacteria. Proc. Natl. Acad. Sci. U.S.A. **119**(33): e2203156119. doi:10.1073/pnas.2203156119. PMID: 35943982.
- von Kügelgen, A., van Dorst, S., Yamashita, K., Sexton, D.L., Tocheva, E.I., Murshudov, G., et al. 2023. Interdigitated immunoglobulin arrays form the hyperstable surface layer of the extremophilic bacterium *Deinococcus radiodurans*. Proc. Natl. Acad. Sci. U.S.A. **120**(16): e2215808120. doi:10.1073/pnas.2215808120. PMID: 37043530.
- Voss, N.R., and Gerstein, M. 2010. 3V: cavity, channel and cleft volume calculator and extractor. Nucleic Acids Res. **38**(Web Server issue): W555–W562. doi:10.1093/nar/gkq395. PMID: 20478824.
- Woese, C.R., Stackebrandt, E., Macke, T.J., and Fox, G.E. 1985. A phylogenetic definition of the major eubacterial taxa. Syst. Appl. Microbiol. **6**: 143–151. doi:10.1016/s0723-2020(85)80047-3. PMID: 11542017.
- Yu, J., Li, T., Dai, S., Weng, Y., Li, J., Li, Q., et al. 2017. A tamB homolog is involved in maintenance of cell envelope integrity and stress resistance of *Deinococcus radiodurans*. Sci. Rep. **7**: 45929. doi:10.1038/srep45929. PMID: 28383523.